Steel and Composite Structures, *Vol. 14, No. 5 (2013) 473-491*
DOI: http://dx.doi.org/10.12989/scs.2013.14.5.473

Compressive performance with variation of yield strength and width-thickness ratio for steel plate-concrete wall structures

Byong-Jeong Choi[1], Won-Ki Kim[2], Woo-Bum Kim[3] and Cheol-Kyu Kang[*1]

[1]Department of Plant Architectural Engineering, Kyonggi University, 154-42 Gwanggyosan-ro, Yeongtong-Gu, Suwon-Si, Kyonggi-Do 443-760, Republic of Korea
[2]Department of Architectural Engineering, Hoseo University, 20 Hoseo-ro 79bean-gil, Baebang-Eup, Asan-Si, Chungcheongnam-Do 336-795, Republic of Korea
[3]Department of Architectural Engineering, Kongju National University, 56 Gongjudaehak-ro, Gongju-Si Chungcheongnam-Do 314-701, Republic of Korea

(Received April 26, 2012, Revised April 23, 2013, Accepted May 02, 2013)

Abstract. The primary objectives of this paper are to describe the buckling patterns and to determine the squash load of steel plate-concrete (SC) walls. The major variables in this study were the width-thickness (B/t) ratio and yield strength of surface steel plates. Six SC walls were tested, and the results include the maximum strength, buckling pattern of steel plates, strength of headed studs, and behavior of headed studs. Based on the test results, the effects of the B/t ratio on the compressive strength are also discussed. The paper also presents recommended effective length coefficients and discusses the effects of varying the yield strength of the steel plate, and the effects of headed studs on the performance of SC structures based on the test results and analysis.

Keywords: buckling; steel plate-concrete structure; B/t ratio; effective length factor; headed studs; SC structures

1. Introduction

Interest in steel plate-concrete (SC) structures is currently increasing in nuclear engineering structure. A primary reason for this interest is the need to reduce construction duration and cost of nuclear facilities. A number of researchers are actively working on SC structures (McKinley 2002, Liang 2006, Loov 1998, Han 2002, Tao 2008, and Vrcelj *et al*. 2002). Earlier related research was conducted by Uy (Uy 2001) on concrete filled high strength steel box columns. A seven-story dormitory building located in England was constructed using the English Bi-Steel structural system that is similar to SC structures. A number of researchers from Japan have performed compression tests on SC walls and have provided an empirical formula for compressive strength (Kanchi *et al*. 1996). However, the number of past test specimens subjected to compressive loading is limited. Accordingly, in this study, a series of compression tests was conducted to further investigate the compressive strength of SC walls. The paper represents the results of the compression tests and of the analysis of the relationship between the width-thickness (B/t) ratio of

∗Corresponding author, Assistant Professor (Ph.D.), E-mail: steel999@kgu.ac.kr

http://www.techno-press.org/?journal=scs&subpage=8 ISSN: 1229-9367 (Print), 1598-6233 (Online)

the steel plates and the spacing of adjacent headed studs on compressive strength. This paper also examines the compression characteristics, and the buckling behavior of the steel plates with the aim of providing practical design guidance.

2. Backgrounds and issues

SC structures can take many forms. In general, however, SC structures consist of a series of interconnected SC wall and floor elements. SC wall elements generally consist of a pair of steel plates with concrete cast between the plates. Normally, no reinforcing bars are placed in the concrete, as the outer steel plates serve both as formwork for the concrete and as reinforcement. Headed studs are typically provided on the inner surface of the steel plates to permit the development of composite action. SC structures were originally developed in Japan to be used in nuclear power plants. Compared to more conventional reinforced concrete or composite structures, SC structures hold the promise of more rapid construction and reduced cost by eliminating the need for formwork.

Researchers in Japan performed a series of compression tests using SC wall structures, and evaluated the squash load (Miyauchi *et al*. 1996, Takeuchi *et al*. 1998). They studied the maximum compressive strength of the walls, the load-sharing relationship between the steel plate and the concrete, the failure shape in relation to the steel plate B/t ratio, and the strength of the headed studs. Based on these researches, AIJ suggested Eq. (1) to estimate the compressive strength of an SC walls, as follows (AIJ 2005).

$$P_n = P_c + P_{sf} + P_{si} = A_c F_{ck} + A_s F_{cr} + A_{si} F_{yi} \tag{1}$$

where, p_n is the nominal compressive strength of the SC wall, A_c is the area of the concrete, A_s is the area of the surface steel plate, A_{si} is the area of the side steel plate, F_{ck} is the concrete compressive strength, F_{cr} is the local buckling stress of the surface steel plate and F_{yi} is the yield strength of the side steel plate in the SC structure. In Eq. (1), the local buckling stress of the surface steel plate is estimated as follows.

$$\text{(a) when } B/t \le 600/\sqrt{F_y} : F_{cr} = F_y \tag{2}$$

$$\text{(b) when } B/t \succ 600/\sqrt{F_y} : F_{cr} = F_e \quad \text{where, } F_e = \frac{\pi^2 E}{12K^2 (B/t)^2} \tag{3}$$

where, K is the coefficient of effective length factor in Euler column theory.

Compressive strength predicted by Eq. (1), compared well with experimental results for SC walls constructed with SM 490 steel (similar to ASTM A572 Grade 50). However, the strength predicted by Eq. (1) did not compare as well with experiments on SC walls constructed with SS400 steel plates (similar to ASTM A36). For this case, the experimentally measured compressive strengths were in the range of 83% to 87% of strength predicted by Eq. (1). Thus, further evaluation and possible changes to Eq. (1) are needed to develop more accurate and conservative predictions of the compressive strength of SC walls.

When a SC wall is subject to compression, the steel plates can buckle between the headed studs in horizontal direction. An important issue in predicting buckling of the steel plates is to set the coefficient of the effective length factor between the headed studs. One approach to predicting the buckling strength of the steel plates is to treat the plate as a column with a length equal to the distance between headed studs. With this approach, the elastic buckling stress can be computed with Euler's Eq. (4), as follows.

$$\sigma_{cr-col} = \frac{E\pi^2}{12K^2(B/t)^2} \tag{4}$$

Thus, the length of the plate is taken as the distance B between headed studs, and radius of gyration can be computed as $[(Bt^3/12)/(Bt)]$, where t is the thickness of the plate. In applying Eq. (4), the key issue is the value of the effective length factor K. The research described in this paper evaluated effective length factors through the use of experiments and analysis. Note that Eq. (4) is for elastic buckling only. Predictions for inelastic buckling of the steel plates between headed studs were also studied in this research.

In addition to evaluating effective buckling length, the effects of varying the yield strength of the steel plates and the effects of the tension behavior of the headed studs on compressive strength of SC walls are also discussed in this paper.

3. Experimental test

Six SC wall specimens were tested in compression in this experiment. The test specimens were designed to represent a short length of an SC wall structures to prevent the global buckling. The test setup and specimens were designed so that no rotation was permitted at the top and bottom of the specimen. One of the most important test variables in the experiments was the slenderness ratio (B/t) of the outer steel plates. The unsupported length of the steel plates, B, is the distance between headed studs, and the thickness of the plate is t. In order to prevent the elastic local buckling, AISC requires the width-to-thickness ratio (b/t) of the steel plate not exceeded the limit value: $b/t = 3.76\sqrt{E_s/F_y}$ for compact section (LRFD-2005). On the other hand, EC4 specifies an allowable b/t limit as follows: $b/t = 52\sqrt{235/F_y}$, where (F_y) is in MPa. In AISC, the b/t limit ratio was derived based on the local buckling stress of the steel hollow section, which was equivalent to the yield stress of the steel material. It should also be remembered that the specifications in the codes (EC4, AISC, and ACI) excluded the effect of in-filled concrete, the slenderness limit of the steel hollow section (Liu *et al*. 2003). Also, we should note that there is no slenderness limitation for this type of composite SC structures. We need to introduce the constant of spacing (B) of stud bolts. This is somewhat different from the b/t ratio preventing elastic local buckling. In SC structures the buckling failure of surface steel plates will be governed by the spacing of the stud bolts and it is expressed by Eq. (4).

In the experiments, test specimens were designed with three different B/t values of 25, 33, and 50. These values were selected to allow study of external steel plates over a range of elastic to inelastic buckling behaviors. Specimens with B/t ratio = 50 are expected to buckle within the elastic range. The specimens with B/t = 33 were at the borderline between the elastic and inelastic buckling, and the specimens with B/t = 25 were expected to buckle in the inelastic range. The compressive strength of the concrete was 42 MPa. For a surface steel plate, two different grades of steel were used: SM490 and SS400. The steel plates were 6 mm thick, and the headed studs had a diameter of 9 mm with a length of 71 mm.

Table 1 shows the general schedule of the six test specimens. Specimens No. 1 and No. 4 were normally identical with the same overall size and the same B/t ratios, with the exception that Specimen 1 used SM490 steel plates whereas specimen 4 used SS 400 steel plates. Similarly, Specimens 2 and 5, and Specimen 3 and 6 were nominally identical, except for the grade of steel used for the external plates. Details of the Specimens 2 and 5 are shown in Fig. 1. As can be seen in Fig. 1, the headed studs were installed on the inner surfaces of both steel plates. For Specimens 2 and 5, the headed studs were spaced at 200 mm in the vertical direction, i.e., B = 200 mm to provide B/t = 33.

The headed studs were also installed at the top and bottom plates to prevent an initial slip and to distribute the compression force evenly during the loading phase. The top plate was perforated with tiny air and oval-shaped holes to place the concrete into the specimens. After pouring the concrete, these holes were filled with high strength non-shrinkage mortar.

Compression loading was applied monotonically at the top of the specimens using a universal testing machine with a 10,000 kN capacity. The vertical displacement of the specimens was measured between the end plates using LVDTs located as shown in Fig. 2. The LVDTs were installed to measure the vertical displacement and to check any eccentricity at the initial loading phase. LVDTs were installed at the four corners of the specimen. Strain gauges were attached on the steel plate midway between lines of headed studs shown in Fig. 3. Twelve strain gauges were attached to the surface steel plates on each specimen so that the buckling could be detected. The

Table 1 Test series of the wall specimen

No.	Specimen	B/t	F_{ck} (MPa)	F_y (MPa)	F_u (MPa)	Dimension (mm) D	W	H	W/D
1	CP35/490 T6.0B50	50	42	418	527	300	680	900	2.27
2	CP35/490-T6.0B33	33					480	600	1.60
3	CP35/490-T6.0B25	25					380	450	1.50
4	CP35/400-T6.0B50	50		274	432		680	900	2.27
5	CP35/400-T6.0B33	33					480	600	1.60
6	CP35/400-T6.0B25	25					380	450	1.50

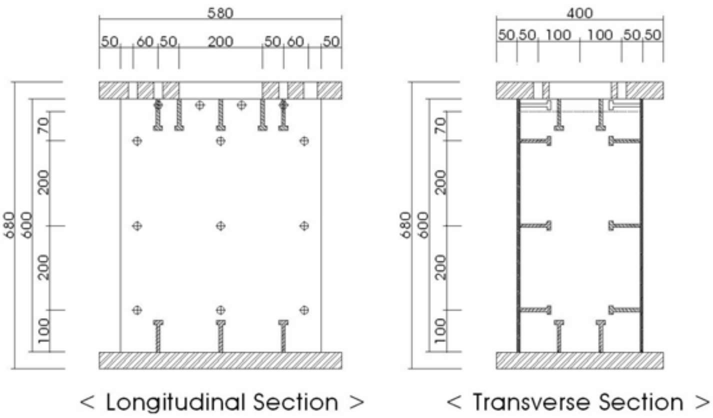

Fig. 1 Details of Specimen 2 and 5

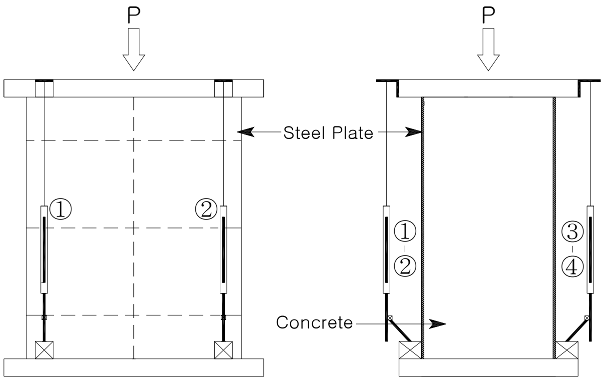

Fig. 2 LVDT locations for test specimens

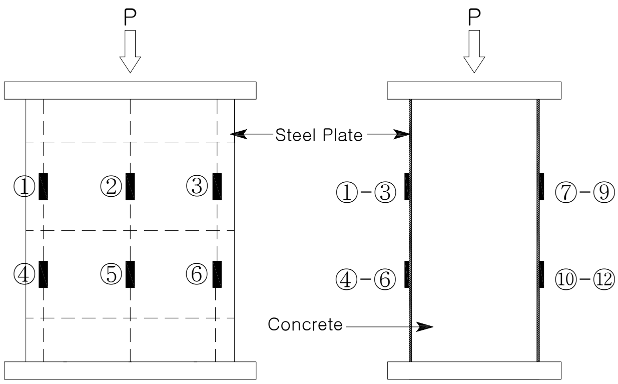

Fig. 3 Strain gauge locations for test specimens

Table 2 Coupon test results for the steel plates (average)

Steel Type	t (mm)	F_y (MPa)	F_u (MPa)	E (MPa)	$\frac{F_y}{F_u}$	B/t limit of steel plate in compression $588/\sqrt{F_y}$
SS 400	6.0	274	432	2.0E5	0.63	35.5
SM490	6.0	418	572	2.0E5	0.73	28.8

strains of concrete were also measured from the installed strain gauge in the center of the specimens. The material properties of the steel plates are shown in Table 2.

4. Analysis and results

4.1 Buckling patterns

The general buckling shapes are shown in Figs. 4 and 5. The buckling shapes for Specimens 1 through 3, in which SM490 steel plates were used, are shown in Fig. 4, and those Specimens 4 through 6, in which SS400 steel plates were used, are shown in Fig. 5. The steel plates in both the front and back surfaces buckled between the transverse lines of the headed studs. Global buckling of the entire specimen did not occur for any of the specimens, due to confining studs and the short length of the specimens. Consequently, local buckling of the steel plates occurred for all specimens, as was desired in this test program. The buckling of the steel plates on the front and back surfaces did not occur at the same location, due to slight eccentricities of the load and construction procedures. The pattern of the buckling shapes of the specimen was very similar each other. The local buckling of the Specimen 1 through 3 occurred at the upper part. The local buckling of the remainder of the specimens also occurred at the upper and middle parts. In other words, the local buckling of all specimens with SM490 steel plate occurred at the upper and middle locations. The buckling patterns of specimen with SS400 steel plates were very similar to those of SM490 specimens. The buckling occurred almost constantly right after yielding of steel plates.

4.2 Maximum compressive strength

This section presents information on the maximum compressive strength of the test specimens. Test results are presented first, followed by comparisons with empirical estimates of compressive strength. Data on the compressive strength of each test specimen is listed in Table 3. This table lists the peak compressive load sustained by each specimen, which is shown at $P_{\max}$. Also listed is the compressive load when buckling of the external steel plates was first observed, which is shown as $P_{local\ buckling}$.

Fig. 4 Buckling patterns for Specimens 1, 2, and 3 (SM490)

Fig. 5 Buckling patterns for Specimens 4, 5, and 6 (SS400)

Table 3 Failure load vs. buckling load of steel plates (kN)

No.	Specimen	P_{max}	$P_{local\ buckling}$		$P_{local\ buckling}/P_{max}$	
			Center	Avg.	Center	Avg.
1	CP35/490-T6.0B50	8850	2986	3031	0.33	0.34
2	CP35/490-T6.0B33	8069	5616	5452	0.7	0.68
3	CP35/490-T6.0B25	6562	5110	5084	0.78	0.77
4	CP35/400-T6.0B50	8956	3858	3850	0.43	0.43
5	CP35/400-T6.0B33	7051	5440	5665	0.77	0.77
6	CP35/400-T6.0B25	6281	5085	5120	0.81	0.82
7	Average Value	-	-	-	0.64	0.69

For each grade of steel, the maximum compressive strengths increased with an increase of the B/t ratio from 25 to 50 because of the overall dimensions of the specimens. For example, the maximum compressive strength of Specimen No. 1 (SM490 steel, B/t = 50) was 8850 kN, and the steel started to yield at a load level of 33% of the maximum compressive strength. On the other hand, the maximum compressive strength of Specimen No. 3 (SM490 steel, B/t = 25) was 6562 kN, and the steel plates started to yield at the load level of 77% of the maximum compressive strength. This means that with the lower B/t ratio, a higher composite behavior was manifested by Specimen No. 3 and No. 6, as can be seen in Table 3. However, numerical comparison of the maximum strengths must also consider that Specimen 1 and 4 were larger than Specimen 3 and 6. Averaged over all six specimens, the test results show that the steel plates started to yield at an average load level of 69% of the maximum compressive strength. The yielding of the steel plates in Specimens No. 3 and No. 6, however, occurred at an average load level that was 79.5% of the maximum compressive strength. This means that, once again, the composite behavior of the steel plates in Specimens No. 3 and No. 6 (B/t =25) was significantly superior to that of the other specimens. It appears that the smaller B/t ratio results in improved strain compatibility between the steel and concrete.

Table 4 provides comparisons of the measured values of compressive strength with the compressive strength predicted using several methods. Column (2) of this table lists the compressive strength values measured in the tests. Column (3) lists the strength predicted using Eq. (1), AIJ. Column (4) lists the strength predicted by Eq. (5), which is described below. As explained earlier, the steel plates of specimen with B/t = 25 resisted well, close to the ultimate load due to the strain-hardening and composite effects. The ultimate compressive strengths of the specimen with B/t =25 were 6,282 kN (SS400) and 6,562 kN (SM490), respectively, as shown in Table 4. The maximum compressive strengths of all the designed specimens were estimated using Eq. (1). It was proven that the safety margin for the estimation of compressive strength was about 2.8%, based on Eq. (1), as shown in Table 4. Especially, if SC structures are to be used mainly in nuclear power plants, the safety margin of 2.8% may not be sufficient.

To provide a more conservative design equation to predict the compressive strength of SC walls, the following Eq. (5) is adopted.

$$P_n = 2A_p F_{cr} + 0.85 f_{ck} A_c \tag{5}$$

where, P_n is the nominal compressive strength of the SC wall, A_p is the area of the steel plate on

Table 4 Comparison of compressive strength (kN)

Specimen Descriptions	P_{max}	Eq. (1)	Eq. (3)	P_{max} / Eq. (1)	P_{max} / Eq. (3)
(1) CP35/490-T6.0B50	8850	9056	7830	97.7	113.0
(2) CP35/490-T6.0B33	8069	7120	6410	113.3	125.8
(3) CP35/490-T6.0B25	6562	6429	5410	102.1	121.3
(4) CP35/400-T6.0B50	8956	9133	7000	98.1	127.9
(5) CP35/400-T6.0B33	7051	7222	5810	97.6	121.3
(6) CP35/400-T6.0B25	6281	5795	4850	108.4	129.5
(7) Average		-	-	102.8	123.1

one side, f_{ck} is the concrete compressive strength, and A_c is the area of the concrete in the SC structure. In Eq. (5) the term, F_{cr}, is used to represent the local bucking stress of the surface steel plates. The primary reason that the local buckling stress, F_{cr}, of steel plate is suggested instead of using F_y is to limit the local buckling of the steel member before yielding in the elastic ranges for nuclear SC structures. Based on the finite element analysis and curve fitting of the analysis results, the local buckling stress of the surface steel plate is adopted as follows (KEA, KEPIC-SNG 2010).

$$F_{cr} = (1.55\text{-}0.043\frac{K\,B}{t}90\varepsilon_n)F_{yf} \prec F_{yf} \tag{6}$$

where, K is the coefficient of effective length factor, B is the distance between headed studs, t is the thickness of the surface steel plate, ε_n is the nominal compressive strain, and F_{yf} is the yield strength of surface steel plate in the SC structure.

By adopting Eq. (5), a safety margin of more than 20-percent is provided between the calculated and experimentally measured strength of the test specimens. It is believed that this level of conservatism is appropriate for the design of nuclear SC structures. Based on the test results, even though the computed value of strength from Eq. (5) is somewhat conservative, it can provide a safe estimate of the compressive strength of SC structures. The coefficient of 0.85 applied to the compressive strength of concrete in Eq. (5) represents the effect of eccentricity and errors in construction. As can be seen in Col. 6 of Table 4, the average safety margin between measured and calculated strength is 23.1% in this study.

4.3 Effects of the B/t ratio and strength increase of steel plate

In the paper, the notation B means the spacing in the horizontal and vertical directions of the headed studs in SC structures. One can install headed studs at different space in horizontal and vertical directions. However, in this paper, the headed studs were spaced at the same distances in both directions. The effects of B/t ratio on the maximum compressive strength of the SM490 steel are shown in Fig. 6.

The initial stiffness was very similar to those of the three specimens. The maximum compressive strength of Specimen No. 1 was higher than those of the other two due to the size of the specimen. However, the maximum compressive strength of Specimen No. 1 was large and showed that steel plates yielded at early phase as we discussed in the previous section. The effects of the B/t ratio on the maximum compressive strength of the SS400 steel are shown in Fig. 7.

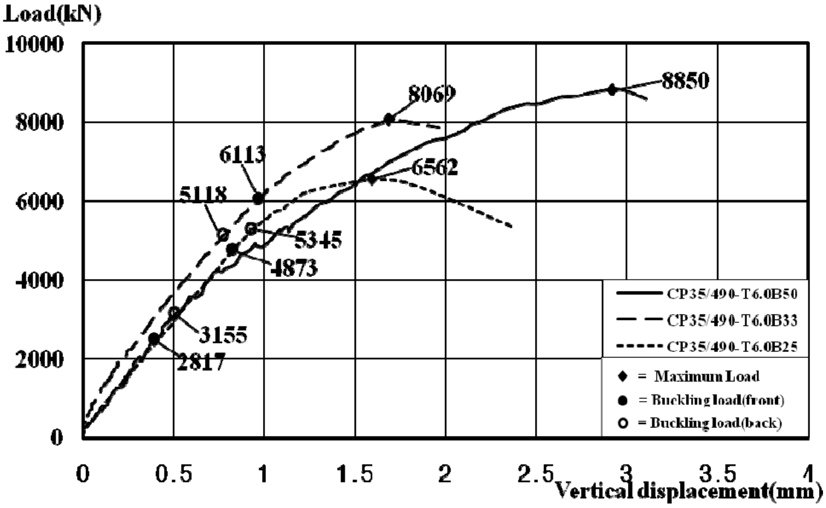

Fig. 6 Effect of B/t ratio on the maximum compressive strength (SM490)

Among all the specimens, Specimen No. 6 is shown to have the lowest compressive strength. The primary reason for this is the size of the specimen.

In this section, the strength index (SI) suggested by Liu (2005) was not considered because the heights of each specimen were different in this type of SC structures. Therefore, the investigation focused on the comparability between the steel plate and concrete to examine the confining effect as follows. The specimens with B/t = 25 were expected to have good composite behavior between the concrete and the steel plate in the SC structures. The specimen with a higher B/t ratio using SM 490 showed poor compatibility in the performance of concrete, as shown in Fig. 8.

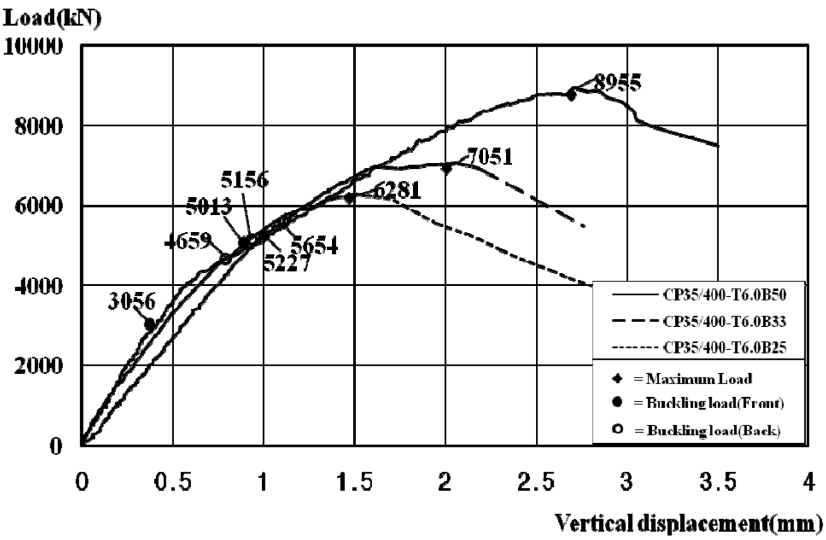

Fig. 7 Effect of B/t ration on the maximum compressive strength (SS400)

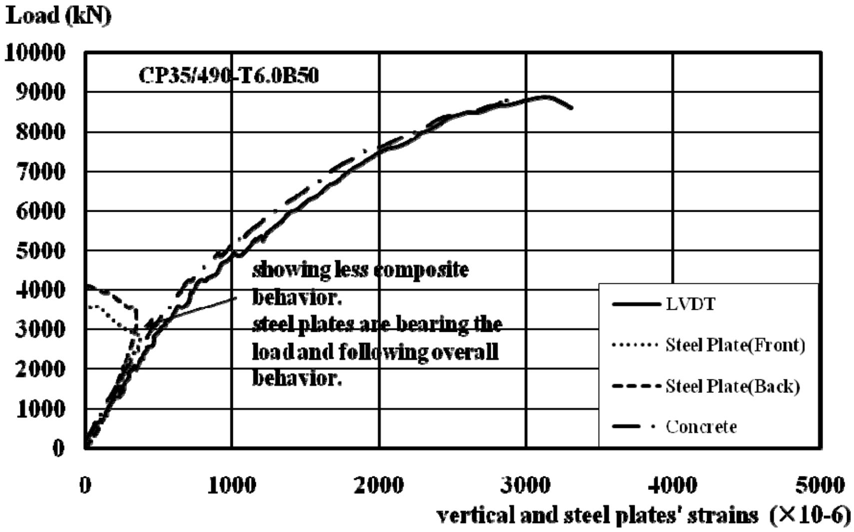

Fig. 8 Compatibility of steel plates against ultimate loading (B/t = 50)

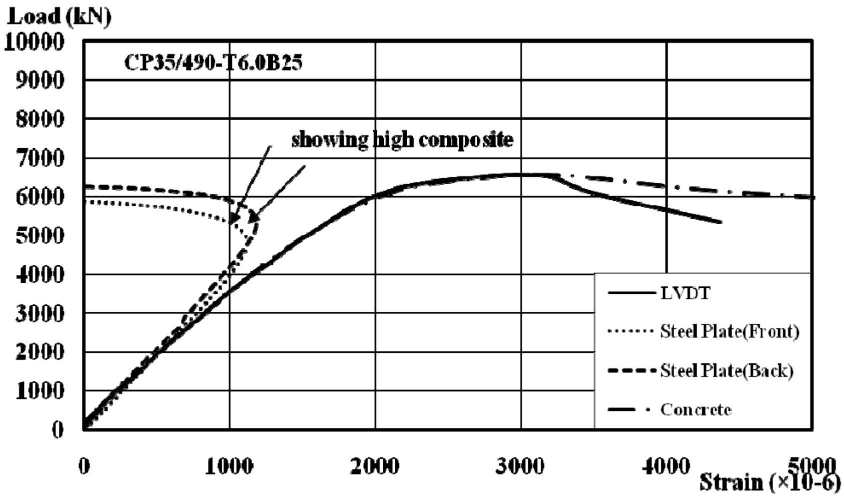

Fig. 9 Compatibility of steel plate against ultimate loading (B/t = 25)

The strain of the concrete was measured in the middle of the specimen and the vertical strain acquired from LVDT. The two strain curves successfully resisted the axial loading onto the ultimate points. The steel plate, however, did not follow the concrete's deformable strain, and failed early.

On the other hand, the specimen with B/t = 25 (No. 3) manifested better behavior in some respects, as shown in Fig. 9. The steel plates sustained well and followed the performance of the concrete due to the effect of the reduced B/t ratio and increased yield strength effects. The results of the comparison of the maximum yield strengths are shown in Figs. 10 and 11. Generally, if the yield strength of a steel plate increases, the compressive strength also increases, as reflected in Eqs. (1) and (5). However, the difference is not clearly shown in the specimen with B/t = 50. The compressive strengths of Specimens No. 1 and No. 4 were 8,850 kN and 8,955 kN, respectively. The loads vs. vertical-displacement curves were very similar from the beginning to the end.

The yield strength effect did not contribute to the increase of the maximum compressive strength for the specimen representing elastic region. The comparisons of the compressive strengths for Specimens No. 2 and No. 5 are shown in Fig. 11. The maximum compressive strength and initial stiffness of Specimen No. 2, which had a higher yield strength (8,069 kN), were higher than those of Specimen No. 5 with lower yield strength (7,051 kN). As shown in Fig. 12, the specimen No. 3 with higher yield strength resulted in higher compressive strength.

The maximum compressive strengths of Specimens No. 3 and No. 6 were shown to be 6,562 kN

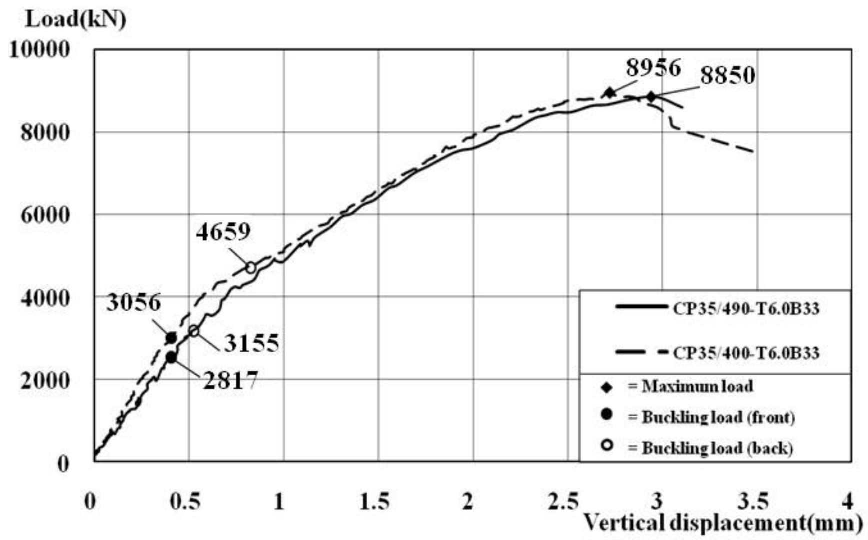

Fig. 10 Effect of yield strength for steel plate with *B*/*t* = 50

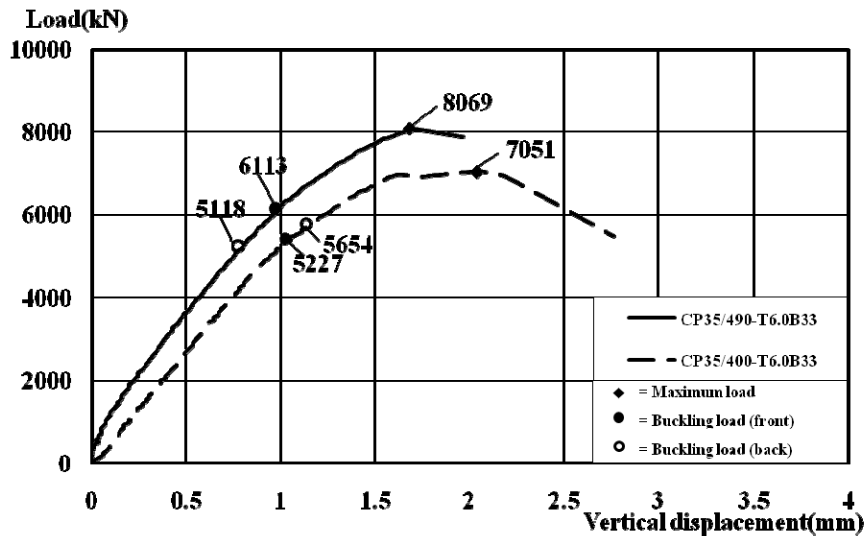

Fig. 11 Effect of yield strength for steel plate with B/t = 33

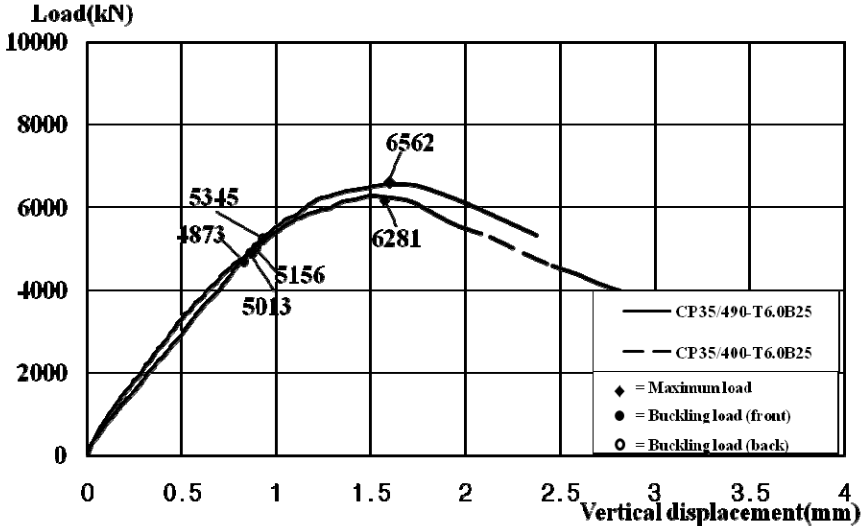

Fig. 12 Effect of yield strength for steel plate with B/t = 25

and 6,281 kN, respectively. It can thus be concluded that an increase in the yield strength seems to increase the maximum compressive strength, as is the case in the increase of the theoretical increment by A_pF_y in Eq. (5), except for the slender specimen. This means that the yield strength of the slender specimen does not affect the compressive strength due to the elastic buckling failure in the elastic region.

4.4 Analysis of the buckling of steel plates

The buckling of a steel plate is a key factor in the decision of the maximum compressive strength of the steel plate. Liu *et al*. (2003) also performed an analysis over a range of column lengths, which involved local buckling and overall flexural buckling using steel hollow section compression members. In this paper, the strain vs. B/t relationship curve was also used to investigate the buckling of surface steel plates confined by headed studs and concrete. Strain gauges were attached to the inner face of all the steel plates. The strains were directly measured from the tests, and the strain values were recalculated using the Euler equation, which represents the elastic-column theory. The Euler equation was modified for the steel plate concrete structures, as can be seen in Eq. (5). The critical yield stress could also be calculated at the same time based on the plate buckling theory, using Eq. (8). The two calculations were compared in this study to find a reasonable estimation method supported by the headed studs in SC structures. Furthermore, the buckling stress of the steel plates at the adjacent headed studs, in a vertical direction, was assumed and calculated based on the column and plate buckling theories (Galambos 1998).

$$\sigma_{cr-col} = [\frac{\pi^2 EI}{(KL)^2}]/Bt = \frac{\pi^2 E}{12K^2(B/t)^2} \tag{7}$$

$$\sigma_{cr-plate} = k_{pl}\frac{\pi^2 E}{12(1-\nu)^2(B/t)^2} \tag{8}$$

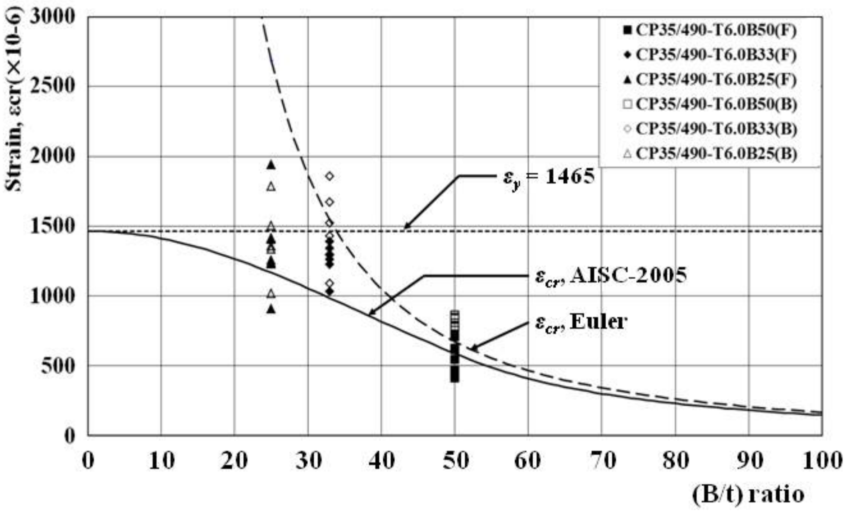

Fig. 13 Strain vs. *B*/*t* ratio of steel plates for SM400 using column analysis

In Eq. (7), *K* is the effective length factor of the steel plates supported by headed studs in the SC structure, and k_{pl} in Eq. (8) is the buckling coefficient of the plate element where the steel plate behaves similarly to a plate supported by four corner studs.

The strain of the steel plates was directly measured from the reading of the test results to calculate the effective length factor in Eq. (7). The buckling strains for the specimens with SS 400 series resulted in values that were somewhat higher than that of the plot by AISC-2005, as shown in Fig. 13. The buckling strains for all the types of *B*/*t* ratios were in the safety regions.

At the same time, the buckling strains with SM490 steel also ranged near the boundary lines of

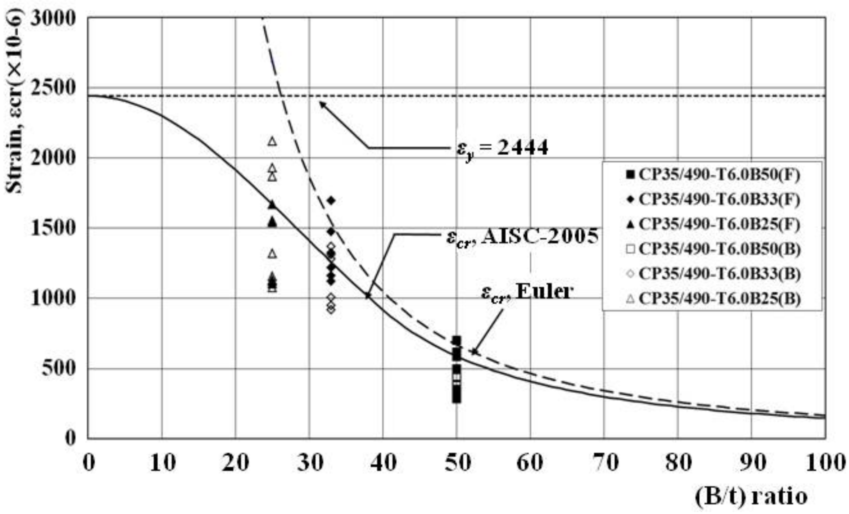

Fig. 14 Strain vs. *B*/*t* ratio for steel plates with SM490 using column analysis

the AISC-2005. The buckling strain dots for the B/t ratio of 50, however, were slightly lower than that of the AISC-2005, as shown in Fig. 14. It must be further investigated, however, and more test results must be obtained for verification purposes.

In the plate buckling theory, the buckling coefficient of the plate elements subjected under axial compression with simply supported condition can be calculated by Eq. (9) with a simple assumption. If we assume $n = 1$ to get the maximum value of the buckling coefficient of the plate elements, Eq. (9) was then rearranged as Eq. (10). Then, Eq. (10) was then inserted into Eq. (8) to get the B/t ratios shown in Figs. 15 and 16.

$$k_{pl} = \left(\frac{m}{\alpha}\right)^2 + 2n^2 + n^4\left(\frac{\alpha}{m}\right)^2 \tag{9}$$

$$k_{pl} = \left(\frac{m}{\alpha} + \frac{\alpha}{m}\right)^2 \tag{10}$$

The buckling strains vs. B/t ratios based on the plate theory are shown in Figs. 15 and 16. The buckling strain of the specimen with lower yield strength, SS400 series (Specimen No. 4, No. 5, and No.6) resulted in dots lower than expected considering its B/t ratio of 25, as shown in Fig. 15. The same pattern occurred to the specimen with SM490 series (Specimens No. 1, 2 and 3) and with a B/t ratio of 25, as shown in Fig. 16. It can thus be summarized that the estimation of the buckling strain of the specimen with a B/t ratio of 25 can be approximated well by the column theory rather than that based on the plate theory. The strains of steel plates of B/t 50 specimen are agreed well under both column theory and plate theory.

4.5 Effective length coefficient

To calculate the effective length coefficient of an SC structure, the column behavior is assumed

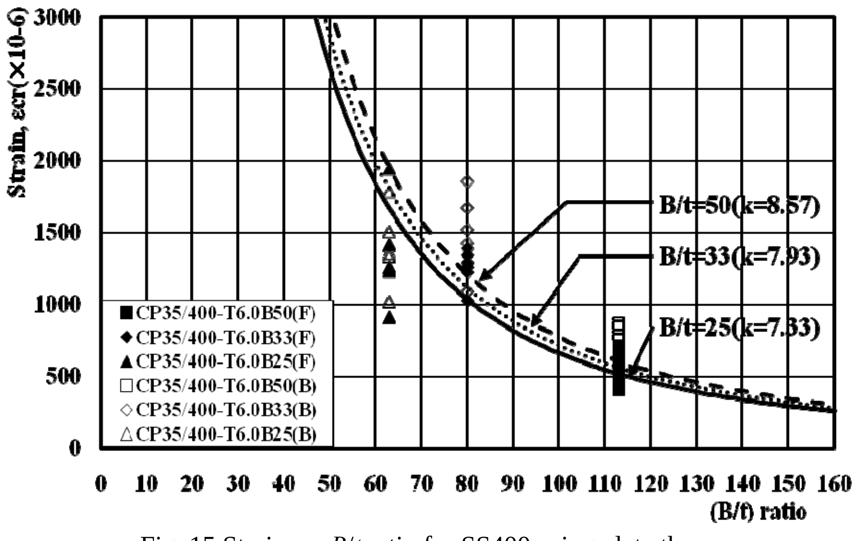

Fig. 15 Strain vs. B/t ratio for SS400 using plate theory

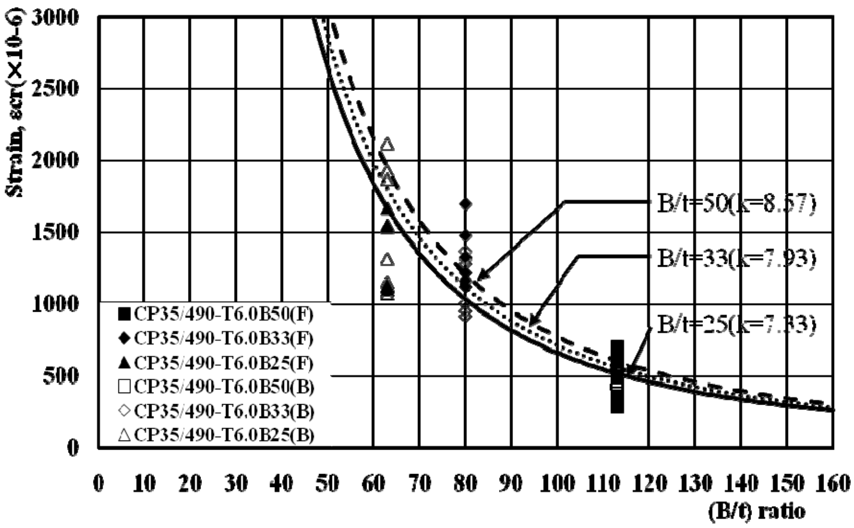

Fig. 16 Strain vs. *B*/*t* ratio for SM490 using plate theory

to be supported by the upper and lower studs in the structure. The effective buckling coefficient can be calculated using the Euler equation, and the buckling strain was measured directly from the strain gauge. The equation for *K* can be rearranged using Eq. (11).

$$K^2 = \frac{\pi^2}{12\varepsilon(B/t)^2} \tag{11}$$

The coefficient *K* represents the effective buckling coefficient of the column plates buckling as column behavior supported by the headed studs at both ends, and the strain ε was measured directly from the strain gauge from the test. The B/t = 25 and 33 specimens were not considered in the calculation of the effective length coefficient. Those two specimens were designed to represent the nonlinear behavior. Thus, the B/t = 50 specimen was used to be evaluated through the elastic Euler equation. The coefficient of effective buckling length, *K*, ranged from 0.62 to 0.74, and the average value was 0.66, which is slightly higher than the one (0.7) from Kanchi (Kanchi *et al*. 1996) shown in Fig. 17.

It is expected that if the steel plate can be stiffened by adding some elements, such as a *W*-shaped rib, the effective stiffness can be further enhanced.

4.6 Tension behavior of studs

If studs are installed on the surface plates under the compression loading, they can exhibit composite behavior. They initially is subjected by shear forces in the elastic region, then transformed into tension forces at the time of beginning of the separation of the concrete and steel plates. In other words, the steel plates at the adjacent stud bolts move outward from the straight surface and the tension force acts on the headed stud bolts. In this case, the maximum elastic compression strength between stud bolts and tension force per headed studs can be expressed

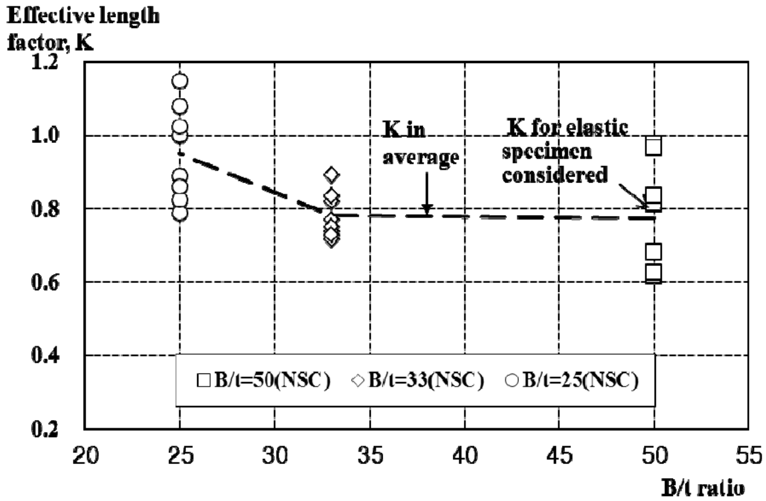

Fig. 17 Effective length factor on B/t ratio

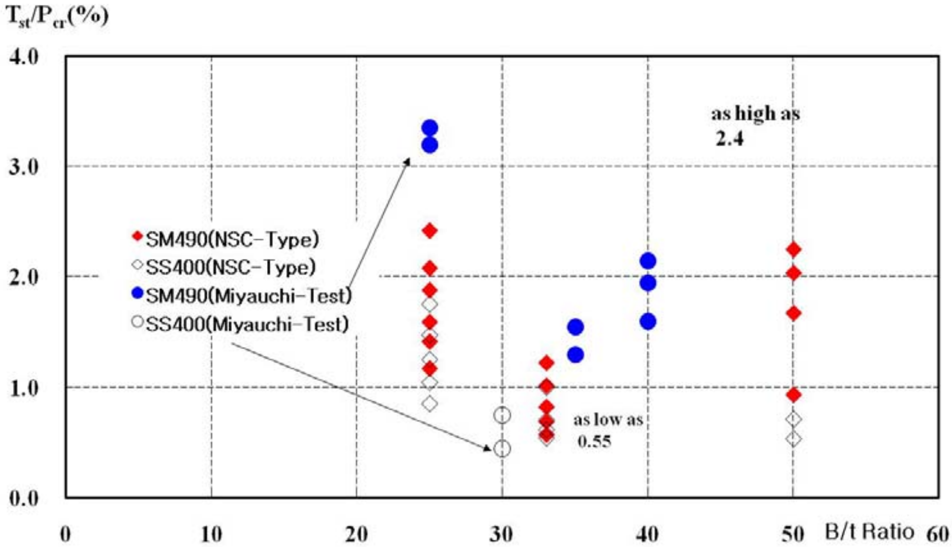

Fig. 18 Normalized ratio of the headed stud bolts with B/t ratio

by Eq. (12) and Eq. (13).

$$P_{cr} = \varepsilon_{cr} E_{sf} Bt \tag{12}$$

$$T_{st} = \varepsilon_{st} E_{st} A_{st} \tag{13}$$

where ε_{cr} is the measured buckling strain of a steel plate, E_{sf} is the elastic modulus of a steel plate, Bt is the area of a steel plate between the studs, ε_{st} is the measured strain from the body of the headed stud bolt, E_{st} is the elastic modulus of the headed stud bolt, and A_{st} is the area of the headed stud bolt.

The buckling strength of the steel plate was calculated in this study using Eq. (12). The ratios T_{st}/P_{cr} are shown in Fig. 18.

The ratios were ranged from 0.55% to 2.4% for the three types of B/t ratios. The B/t ratios obtained, 25 and 33, were quite typical, but the dispersion was very high for the specimen with a B/t ratio of 50, which represents a slender element. These results were close to the one by Miyauchi who acquired ranges of from 0.5% to 3% (Miyauchi 1996).

5. Conclusions

In this paper, results from compression test were presented, with the focus on the performance of SC structures. The general buckling pattern, the maximum compressive strength, the effect of the yield strength of the steel plate, the effective length factor, the buckling strength of the steel plate, and the tension force acting on the headed stud bolt were also investigated. Based on the results, the following conclusions were drawn:

1. The buckling shapes of the SC structures occurred between the adjacent studs and in the longitudinal direction perpendicular to the loading direction. The increase of the yield strength of the steel plates did not significantly increase the maximum compressive strength of the specimen with a higher B/t ratio.
2. The buckling strain of the steel plates for the three- B/t ratio generally well coincides with the plotted curves of AISC LRFD-2005 based on the column theory.
3. The effective buckling length was about 0.66, which is close to the fixed-support condition in the column theory. In SC structures, this coefficient of effective buckling length of that value can be cautiously suggested in design practice.
4. The ratio of the tension force acting on the studs over the compression strength is from 0.5% to 2.4% in the SC structures.

Acknowledgements

This research was accomplished with generous support from the Korea Electric Power Industry RND's "Development of the Modular Construction Method in NNP Structures (SC Structures)" in 2007, which the authors deeply appreciate. This work was supported by Korea Research Foundation Grant funded by Korean Government (KRF2011-0027646 and KRF 2011-0026221). The authors would like to express special thanks to Professor Michael Engelhardt, Civil, Architectural and Environmental Engineering Department, University of Texas at Austin, for his valuable comments and academic supports.

References

AIJ, JEAG 4618 (2005), Technical guidelines for seismic design of steel plate concrete structures: for buildings and structures.

Choi, B.J. and Han, H.S. (2009), "An experiment on compressive profile of the unstiffened steel plate-concrete structures under compression loading", *Steel Compos. Struct., Int. J.*, **9**(6), 519-534.

Dabaon, M.A., El-Boghdadi, M.H. and Hassanein, M.F. (2009), "Experimental investigation on

concrete-filled stainless steel stiffened tubular stub columns", *Eng. Struct.*, **31**(2), 300-307.
Dabaon, M.A., El-Khoriby, S., El-Boghdadi, M.H. and Hassanein, M.F. (2009), "Confinement effect of stiffened and unstiffened concrete-filled stainless steel tubular stub columns", *J. Construct. Steel Res.*, **65**(8-9), 1846-1854.
Galambos, Theodore V. (1998), *Guide to stability criteria for metal structures*, (5th Edition), John Wiley & Sons Inc., USA.
Han L.H. (2002), "Tests on stub columns of concrete-filled RHS sections", *J. Construct. Steel Res.*, **58**(3), 353-372.
Han, L.H., Liu, W. and Yang, Y.F. (2008), "Behavior of thin walled steel tube confined concrete stub columns subjected to axial local compression", *Thin-Walled Struct.*, **46**(2), 155-164.
Kanchi, M., Kitano, C., Sgawara, D. and Hiragawa, K. (1996), "Experimental study on a concrete-filled steel structure, compressive test (1)", *Architectural Institute of Japan Conference - Part 2*, 1071-1072.
Kim, W.B. and Choi, B.J. (2011), "Shear strength of connections between open and closed steel-concrete composite sandwich structures", *Steel Compos. Struct., Int. J.*, **11**(6), 169-181.
Korea Electric Association (KEA) (2010), *Steel-concrete structures (KEPIC-SNG)*, Korea Electric Power Industry code, Seoul, Korea.
Kwon, Y.B., Seo, S.J. and Kang, D.W. (2011), "Prediction of the squash loads of concrete-filled tubular section columns with local buckling", *Thin-Walled Struct.*, **49**(1), 85-93.
Liang, Q.Q., Uy, B. and Richard Liew, J.Y. (2006), "Nonlinear modeling and evaluation of concrete-filled steel tubular columns with local buckling effects", *J. Construct. Steel Res.*, **62**(6), 581-591.
Liu, D., Gho, W.M. and Yuan, J. (2003), "Ultimate capacity of high-strength rectangular concrete-filled steel hollow section stub columns", *J. Construct. Steel Res.*, **59**(12), 1499-1515.
Liu, D. (2005), "Tests on high-strength rectangular concrete-filled steel hollow section stub columns", *J. Construct. Steel Res.*, **61**(7), 902-911.
Liu, Y. and Young, B. (2003), "Buckling of stainless steel square hollow section compression members", *J. Construct. Steel Res.*, **59**(2), 165-177.
Loov, R.E. (1998), "Review of A23.3-94 simplified method of shear design and comparison with results using shear friction", *Can. J. Civil Eng.*, **25**(3), 437-450.
LRFD, AISC (2005), *Load and Resistance Factor Design Specification*, Chicago.
McKinley, B. and Boswell, L.F. (2002), "Behavior of double skin composite construction", *J. Construct. Steel Res.*, **58**(10), 1347-1359.
Miyauchi, Y., Ozaki, M., Doutan, Y., Okiwara, R. and Usami, D. (1996), "Experimental study on a concrete-filled steel structure, compressive test (2)", *Architectural Institute of Japan Conference - Part 2*, 1073-1074
Takeuchi, M., Narikawa, M., Matsuo, I., Hara, K. and Usami, S. (1998), "Study on a concrete-filled structure for nuclear power plants", *Nuclear Eng. Design*, **179**(2), 209-223.
Tao Z., Han L. H. and Wang D. Y. (2008), "Strength and ductility of stiffened thin-walled hollow steel structural stub columns filled with concrete," *Thin-Walled Struct.*, **46**(10), 1113-1128.
Tao, Z., Uy, B., Han, L.H. and Wang, Z.B. (2009), "Analysis and design of concrete-filled stiffened thin-walled steel tubular columns under axial compression," *Thin-Walled Struct.*, **47**(12), 1544-1556.
Uy, B. and Bradford, M.A. (1996), "Elastic local buckling of steel plates in composite steel-concrete members", *Eng. Struct.*, **18**(3), 193-200.
Uy, B. (2001), "Strength of short concrete filled high strength steel box columns", *J. Construct. Steel Res.*, **57**(2), 113-134.
Uy, B., Tao, Z. and Han, L.H. (2011), "Behavior of short and slender concrete-filled stainless steel tubular columns", *J. Construct. Steel Res.*, **67**(2), 360-378.
Vrcelj, Z. and Uy, B. (2002), "Strength of slender concrete-filled steel box columns incorporating local buckling", *J. Construct. Steel Res.*, **58**(2), 275-300.

CC

Nomenclature

A_c	area of the concrete
A_p	area of the steel plate on one side
A_s	area of the surface steel plate
A_{si}	area of the side steel plate
A_{st}	area of the headed stud
B	distance between headed studs
Bt	area of a steel plate between the studs
E_{sf}	the elastic modulus of a steel plate
E_{st}	elastic modulus of the headed stud
F_{ck}	specified compressive strength of concrete
F_{cr}	local buckling stress of the surface steel plate
F_{yf}	yield strength of the surface steel plate
F_{yi}	yield strength of the side steel plate
K	coefficient of effective length factor in Euler column theory
K_{pl}	coefficient of effective length factor in plate buckling theory
t	thickness of the surface steel plate
ε_{cr}	measured buckling strain of a steel plate
ε_n	nominal compressive strain
ε_{st}	measured strain from the body of the headed stud